PAPER

Effects of size and shape of hole defects on mechanical properties of biphenylene: a molecular dynamics study

To cite this article: Shuoyang Xiao *et al* 2024 *Nanotechnology* **35** 485703

IOP Publishing Nanotechnology

Nanotechnology **35** (2024) 485703 (10pp) https://doi.org/10.1088/1361-6528/ad7509

Effects of size and shape of hole defects on mechanical properties of biphenylene: a molecular dynamics study

Shuoyang Xiao[1], Jiannan Hao[2], Tan Shi[3], Jianfeng Jin[4], Bin Wu[1,*] and Qing Peng[2,5,6,*]

[1] School of Physics and Astronomy, Beijing Normal University, Beijing 100875, People's Republic of China
[2] State Key Laboratory of Nonlinear Mechanics, Institute of Mechanics, Chinese Academy of Sciences, Beijing 100190, People's Republic of China
[3] School of Nuclear Science and Technology, Xi'an Jiaotong University, Xi'an 710049, People's Republic of China
[4] School of Materials Science and Engineering, Northeastern University, Shenyang 110819, People's Republic of China
[5] Center of Materials Science and Optoelectronics Engineering, University of Chinese Academy of Sciences, Beijing 100049, People's Republic of China
[6] Guangdong Aerospace Research Academy, Guangzhou 511458, People's Republic of China

E-mail: bwu6@bnu.edu.cn and pengqing@imech.ac.cn

Received 20 March 2024, revised 17 August 2024
Accepted for publication 29 August 2024
Published 10 September 2024

Abstract

The distinctive multi-ring structure and remarkable electrical characteristics of biphenylene render it a material of considerable interest, notably for its prospective utilization as an anode material in lithium-ion batteries. However, understanding the mechanical traits of biphenylene is essential for its application, particularly due to the volumetric fluctuations resulting from lithium ion insertion and extraction during charging and discharging cycles. In this regard, this study investigates the performance of pristine biphenylene and materials embedded with various types of hole defects under uniaxial tension utilizing molecular dynamics simulations. Specifically, from the stress−strain curves, we obtained key mechanical properties, including toughness, strength, Young's modulus and fracture strain. It was observed that various near-circular hole (including circular, square, hexagonal, and octagonal) defects result in remarkably similar properties. A more quantitative scaling analysis revealed that, in comparison with the exact shape of the defect, the area of the defect is more critical for determining the mechanical properties of biphenylene. Our finding might be beneficial to the defect engineering of two-dimensional materials.

Keywords: biphenylene, two-dimensional (2D) material, molecular dynamics, mechanical properties, defects

* Authors to whom any correspondence should be addressed.

1. Introduction

A surge of research on two-dimensional (2D) materials [1–22] has emerged following the successful synthesis of graphene in 2004 [23] due to their exceptional properties [24–27], such as ultrahigh room-temperature carrier mobility, high elastic modulus, and remarkable transparency, which promise great potential in various applications [28], including electronics/-optoelectronics, energy storage [29–32], and sensors.

Biphenylene, a nonbenzenoid 2D carbon allotrope, was successfully synthesized by Fan *et al* [33] in 2021, through dehydrogenation fluorination (HF-zipping) of an intersurface polymer. Biphenylene exhibits the general characteristics of 2D carbon allotropes and has been extensively studied in terms of its mechanical, thermal, optical, and electronic properties. A variety of methods have been employed in this research, including density functional theory (DFT) [34–39], molecular dynamics simulations [34, 40, 41], and machine learning techniques [42]. This intriguing 2D material exhibits a periodic arrangement of four-, six-, and eight-membered rings [43, 44]. Owing to the presence of such large ring structures, which could serve as hosts for storing lithium ions, biphenylene may serve as a superior anode material for lithium-ion batteries [45]. The mechanical properties of biphenylene are of paramount concern because the insertion and extraction of Li ions during the charging and discharging processes would necessarily induce volume changes, which in turn lead to internal stress and strain. Therefore, in addition to fundamental material properties, extreme conditions such as fracture are also of great importance [46, 47]. In this regard, Luo *et al* analyzed the structural, mechanical, electronic, and hydrogen evolution reaction properties of biphenylene via first-principles calculations [34]. Pereira *et al* [48] employed reactive molecular dynamics simulations to explore the mechanical properties and fracture patterns of non-defective and defective biphenylene, showing distinct fracture processes and high mechanical resilience. Samadian *et al* [41] used molecular dynamic and DFT simulations to examine the pinhole effect on the mechanical properties of biphenylene nanosheets, concluding that biphenylene has more strength in the zigzag direction and that multiple symmetrical pinholes lead to a greater decline in strength.

However, to the best of our knowledge, there has not been a comprehensive investigation into how defects of various shapes affect the mechanical properties of biphenylene. Gaining insights into this aspect would be highly valuable for the practical deployment and performance of biphenylene and analogous materials in various operational and extreme conditions [49–62]. In this paper, we utilized molecular dynamics simulations to explore the mechanical properties of biphenylene under uniaxial tension. We obtained the toughness, strength, Young's modulus and fracture strain of pristine biphenylene and those containing defects. Furthermore, we examined the influence of the shape and size of the defects on the mechanical properties of biphenylene.

2. Methods

We had carried out molecular dynamics simulations using LAMMPS [63] and visualized structures by ATOMSK and VESTA softwares [64, 65]. As shown in figure 1, the initial structure of pristine biphenylene was replicated from the unit cell containing six atoms. The interatomic potential is described by the AIREBO-Morse pair potential [66–68], which is widely used and validated in simulating carbon-based systems such as graphene, carbon nanotubes and organic molecules[69]. The C–C bond distances are 1.46 Å and 1.45 Å (C1–C1 bond), 1.41 Å (C1–C2 bond) and 1.45 Å (C2–C2 bond), respectively, which agrees well with previous works employed DFT [34], reaxFF potential [48], and AIREBO potential (same as this study) [41]. The hole defects are positioned in the center of the system and are introduced through systematic removal of the relevant atoms based on geometries including the circle, square, hexagon, and octagon. Periodic boundary conditions are applied to all three Cartesian dimensions. Note that the size of the simulation box in the Z direction is as large as 10 nm, which ensures that there is no interaction between two adjacent planes. All the tested systems are relaxed under the NPT ensemble with $P = 0$ atm and $T = 300$ K for 40 000 ps. Then the boxes are stretched along the X direction (zigzag) for mechanical simulations, which has been confirmed to be the direction of maximum strength through molecular dynamics and DFT simulations [34]. In the following, we first investigated the effects of size, temperature, and strain rate on pristine biphenylene. The final box size used to calculate the effect of the defect on the mechanical properties is the same as that in figure 1 with an equivalent defect concentration of 0.025 nm^{-2}. Afterward, the dependence of the mechanical properties on the size and shape of the hole defects was assessed.

To quantify the mechanical performance, we focused on the stress−strain curves throughout the stretching process and derived toughness, strength, Young's modulus and fracture strain. The Young's modulus is defined by the initial slope of the stress−strain curve; the strength corresponds to the maximum stress value during the tensile process, and the fracture strain corresponds to the strain at the point of sharp stress drop, indicating the onset of mechanical failure. Last, the toughness corresponds to the area beneath the stress−strain curve, which characterizes the total mechanical energy absorbed by the material from the initial application of stretching to the final failure.

3. Results

3.1. Size effect

The calculation results derived from molecular dynamics simulations may depend on the size of the system under examination, which is recognized as the size effect. We assessed this effect by performing uniaxial stretching on pristine biphenylene of various dimensions. Specifically, the size of the

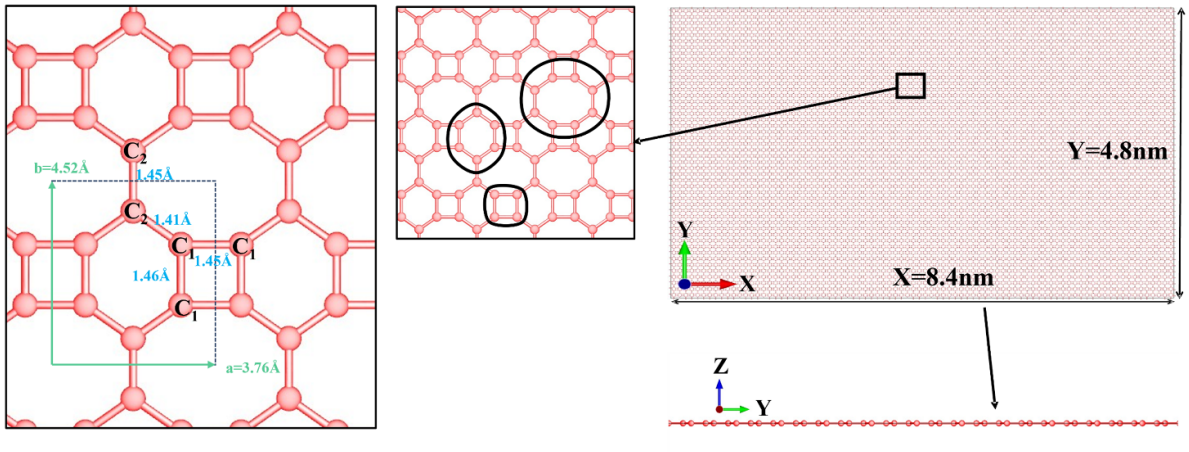

Figure 1. Schematic model of pristine biphenylene using a ball-and-stick representation. As an example, the depicted model measures 8.4 nm in the *X* direction and 4.8 nm in the *Y* direction, totaling 24 192 atoms. Note that biphenylene is composed solely of carbon atoms and that there are square, hexagonal, and octagonal rings in its structure. The primitive cell is marked by black dashed lines, each containing six carbon atoms. Bond length information is denoted in blue, while the lattice constant is indicated in green. The model was visualized using ATOMSK and VESTA software.

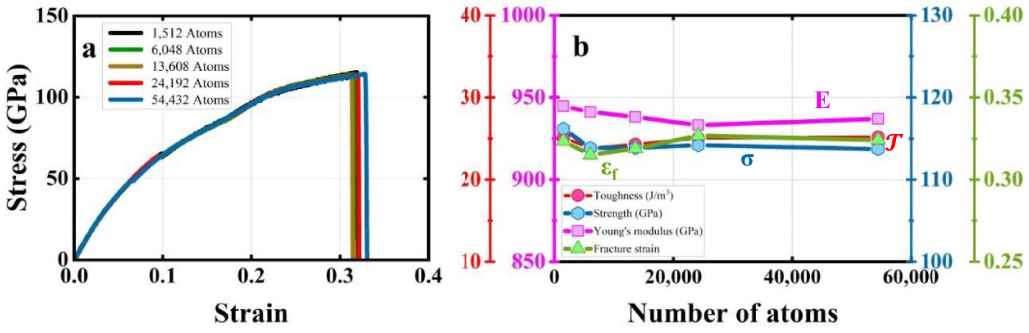

Figure 2. Size effect of simulation results on the mechanical performance of the pristine biphenylene under uniaxial stretching, where the temperature, external pressure, and strain rate are set to 300 K, 0 atm, and 10^9 s^{-1}, respectively. The tested system sizes include 1512, 6048, 13 608, 24 192, and 54 432 atoms. panel (a) shows the stress−strain curves, while panel (b) demonstrates the derived quantities including toughness, strength, Young's modulus and fracture strain.

system ranges from 2.1 nm × 1.2 nm to 12.6 nm × 7.2 nm, where the number of atoms in the enclosure ranges from 1512 to 54 432. Note that the aspect ratio between the Y and X dimensions is set to be fixed for the sake of simplicity. We set the temperature to 300 K and the pressure to 0 atm and applied a strain rate of 1×10^9 s^{-1}. The derived calculation results are depicted in figure 2, where panel (a) shows the stress−strain curves and panel (b) shows the size dependence of the toughness, strength, Young's modulus, and fracture strain.

One sees that the size dependence is rather weak. In panel (a), all the stress−strain curves almost collapse together at low strain; there is a discernible deviation between the various curves around the vicinity of the sharp stress drop. In panel (b), although the derived parameters tend to exhibit small fluctuations in response to variations in the system size, they appear to converge quickly beyond twenty thousand atoms. Furthermore, in addition to the size effect, statistical fluctuations may also contribute to the variation in these observed quantities. Hence, we consider that the system corresponding to 24 192 atoms should suffice to suppress the size effect and thus be employed for the remainder of this study.

3.2. *Temperature effect*

The mechanical performances of pristine biphenylene at various temperatures ranging between 200 K and 600 K are illustrated in figure 3. The strain rate is fixed at 1×10^9 s^{-1}. In panel (a), one sees that the stress−strain curves systematically shift toward the left with increasing temperature. In panel (b), the derived quantities, including toughness, strength, Young's modulus, and fracture strain decrease monotonically in response to increasing temperature. These observations

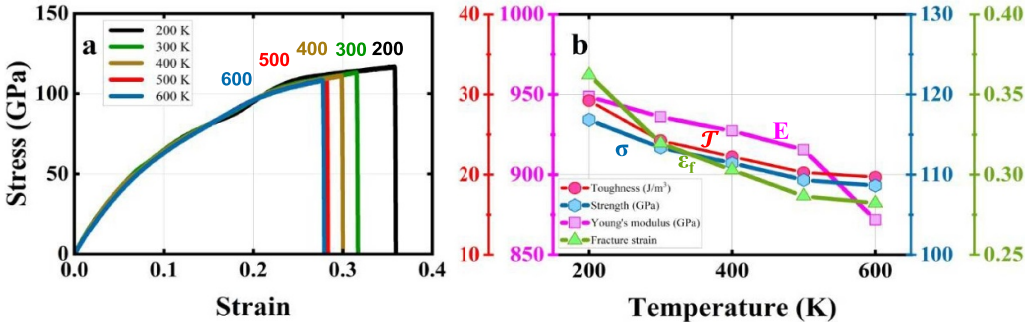

Figure 3. Temperature effect on the mechanical performance of the pristine biphenylene under uniaxial stretching, where the external pressure and strain rate are set to 0 atm and 1×10^9 s^{-1}, respectively. The test temperatures include 200, 300, 400, 500, and 600 K. panel (a) shows the stress−strain curves, while panel (b) demonstrates the derived quantities including toughness, strength, Young's modulus and fracture strain.

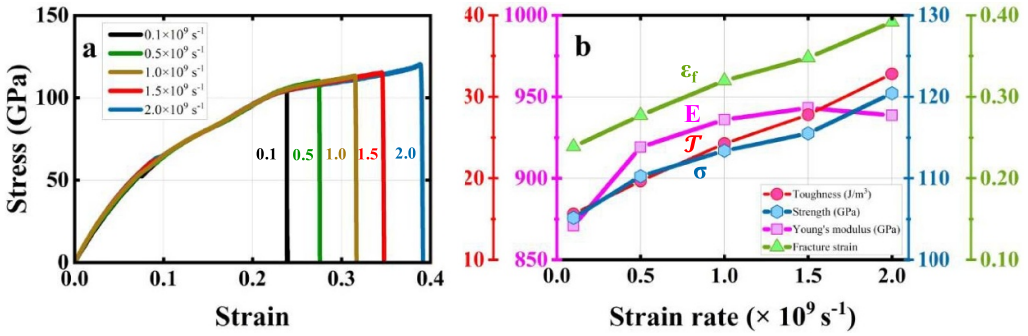

Figure 4. Strain rate effect on the mechanical performance of the pristine biphenylene under uniaxial stretching, where the external pressure and temperature are set to 0 atm and 300 K, respectively. The concerned strain rates include 0.1, 0.5, 1.0, 1.5, and 2.0×10^9 s^{-1}. panel (a) shows the stress−strain curves, while panel (b) demonstrates the derived quantities including toughness, strength, Young's modulus, and fracture strain.

suggest that an increase in temperature leads to mechanical softening of biphenylene.

3.3. Strain rate effect

The dependences of the mechanical properties on the strain rate are demonstrated in figure 4. The considered strain rates range from 0.1×10^9 s^{-1} to 2.0×10^9 s^{-1}. In panel (a), the stress−strain curves shift to the right in response to increasing strain rate. In panel (b), the derived quantities, including toughness, strength and fracture strain, monotonically increase with increasing strain rate; nonetheless, Young's modulus seems to converge at strain rates greater than 1.0×10^9 s^{-1}. It is understandable that the experimentally accessible strain rates are outside the scope of molecular dynamics simulations and are orders of magnitude lower than those from the present study. Hence, one can infer that the simulation results presented herein may overestimate the mechanical properties of pristine biphenylene at the experimental scale [70–72].

3.4. Impact of hole defects

We investigated the impact of the shape and size of hole defects on the mechanical properties of biphenylene. The shapes under examination include circles and several polygons, namely, squares, hexagons, and octagons. Figure 5 shows the dimensional description of biphenylenes with different shaped holes: L_c is the diameter of the circular hole, L_s is the side length of the square hole, L_h is the distance between the two farthest points of the hexagon hole, and L_o is the distance between the opposite sides of the octagonal hole.

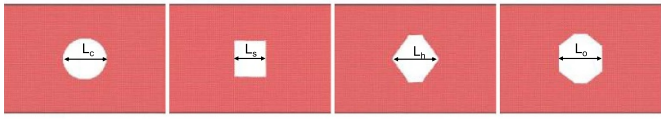

Figure 5. The dimensions of the different shapes of biphenylene are indicated as follows: L_c represents the diameter of the circular hole, L_s represents the side length of the square hole, L_h represents the distance between the two farthest points of the hexagon, and $_oL$ represents the opposite side distance of the octagonal hole.

3.4.1. Circular hole. The size of the circular hole is quantified by the hole diameter, denoted as L_c, which ranges from 0.6 nm to 2.2 nm. The simulation results are illustrated in figure 6. In panel (a), one sees that the stress−strain curves systematically become shorter and narrower with increasing

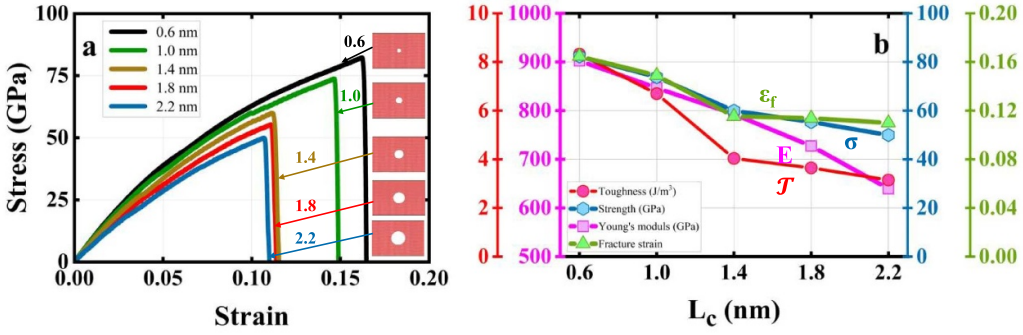

Figure 6. Mechanical performance of biphenylene embedded with circular hole defects under uniaxial stretching, where the temperature, external pressure, and strain rate are set to 300 K, 0 atm, and 1×10^9 s^{-1}, respectively. The hole diameters of interest are 0.6 nm, 1.0 nm, 1.4 nm, 1.8 nm, and 2.2 nm. panel (a) shows the stress−strain curves, while panel (b) shows the derived quantities, including toughness, strength, Young's modulus and fracture strain.

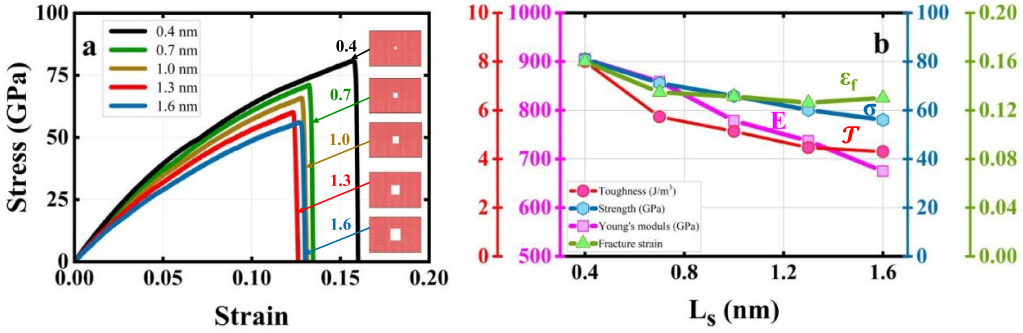

Figure 7. Mechanical performance of biphenylene embedded with square defects under uniaxial stretching, where the temperature, external pressure, and strain rate are set to 300 K, 0 atm, and 1×10^9 s^{-1}, respectively. The relevant square dimensions, denoted L_s, are 0.4 nm, 0.7 nm, 1.0 nm, 1.3 nm, and 1.6 nm. panel (a) shows the stress−strain curves, while panel (b) shows the derived quantities, including toughness, strength, Young's modulus and fracture strain.

hole diameter, suggesting a gradual deterioration of the mechanical properties. Specifically, Young's modulus, reflected by the slope of the stress−strain curves, decreases almost linearly with increasing hole diameter. However, the evolution of toughness, strength and fracture strain shows nonlinear dependences: there is a sharp decrease in these quantities when the hole diameter is smaller than 1.4 nm, after which the changes subsequently become sluggish. The inner edge of the circle transitions from 'rough' to 'smooth'. At the atomic scale, smaller circles are polygons, and only become approximately circular as they increase in size, hence the mechanical properties show a segmented performance. For instance, the fracture strain decreases from 0.165 to 0.115 when the hole diameter increases from 0.6 nm to 1.4 nm, whereas it decreases from 0.115 to 0.110 when the hole diameter increases from 1.4 nm to 2.2 nm. The evolutions of toughness and strength are qualitatively similar to that of fracture strain.

3.4.2. Polygonal hole. The polygonal holes under consideration include squares, hexagons, and octagons. The size of the square is measured by the side length, denoted $_s$, L which ranges from 0.4 nm to 1.6 nm; the dimension of the hexagon is quantified by the farthest distance between any two vertices, denoted L_h, which ranges from 0.8 nm to 2.4 nm; and the size of the octagon is represented by the distance between two parallel sides, denoted L_o, which ranges from 0.6 nm to 2.2 nm.

The simulation results are presented in figures 7–9. The evolutions of the stress−strain curves and the derived quantities, namely, toughness, strength, Young's modulus, and fracture strain, in response to the variation in defect size are qualitatively similar to those from circular defects. The stress−strain curves become increasingly shorter with increasing defect size. Moreover, the Young's modulus shows a linear dependence on the dimension of the defect. In contrast, the toughness, strength, and fracture strain exhibit nonlinear dependences. Taking the fracture strain as an example, for square-shaped defects, it decreases from 0.160 to 0.131 when L_s increases from 0.4 nm to 0.7 nm, whereas it decreases from 0.131 to 0.126 when L_s increases from 0.7 nm to 1.0 nm; for hexagon-shaped defects, it decreases from 0.147 to 0.122 when L_h increases from 0.8 nm to 1.2 nm, whereas it decreases from 0.122 to 0.112 when L_h increases from 1.2 nm to 1.6 nm; for octagon-shaped defects, it decreases from 0.14 to 0.12 when L_o increases from 0.6 nm to 1.8 nm, whereas it decreases from 0.12 to 0.1 when L_o increases from 1.8 nm to 2.2 nm.

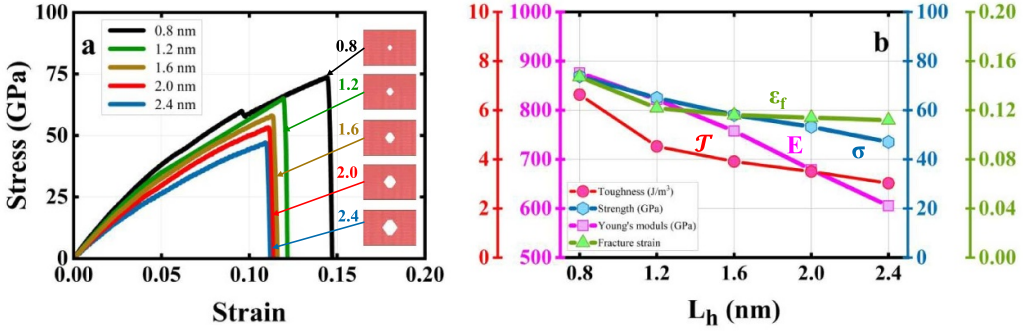

Figure 8. Mechanical performance of biphenylene embedded with hexagonal defects under uniaxial stretching, where the temperature, external pressure, and strain rate are set to 300 K, 0 atm, and 1×10^9 s^{-1}, respectively. The hexagon dimensions, denoted L_h, are 0.8 nm, 1.2 nm, 1.6 nm, 2.0 nm, and 2.4 nm. panel (a) shows the stress−strain curves, while panel (b) shows the derived quantities, including toughness, strength, Young's modulus and fracture strain.

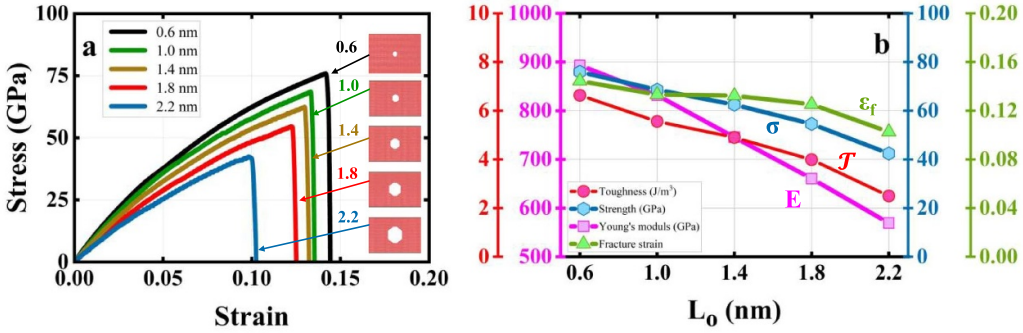

Figure 9. Mechanical performance of biphenylene embedded with octagonal defects under uniaxial stretching, where the temperature, external pressure, and strain rate are set to 300 K, 0 atm, and 1×10^9 s^{-1}, respectively. The octagon dimensions, denoted L_o, are 0.6 nm, 1.0 nm, 1.4 nm, 1.8 nm, and 2.2 nm. panel (a) shows the stress−strain curves, while panel (b) shows the derived quantities, including toughness, strength, Young's modulus and fracture strain.

4. Discussion

First, we compare the mechanical properties of biphenylene against those of other common 2D materials [73–80]. The comparisons are illustrated in figure 10. Biphenylene has excellent mechanical properties among all the listed 2D materials and is comparable to graphene.

Second, we investigated the fracture mechanism by monitoring the stress evolution at the atomistic level throughout the stretching process. The calculation results are illustrated in figure 11, where each row corresponds to one type of defect with an exemplary size, while each column corresponds to a specific strain state. Note that the first three columns are at the same strain states, namely, 0, 0.05, and 0.1, respectively, while the fourth and fifth columns are at the immediate onset and aftermath of the stress drop for each specific case. The stress gradually increases with increasing strain. Furthermore, stress is concentrated on the perimeter of the hole along the direction that is perpendicular to that of stretching. In the fourth column, one sees the emergence of a small crack emanating from the stress-concentrated perimeter, and the crack becomes wider in the fifth column, signifying the failure of the material. Hence,

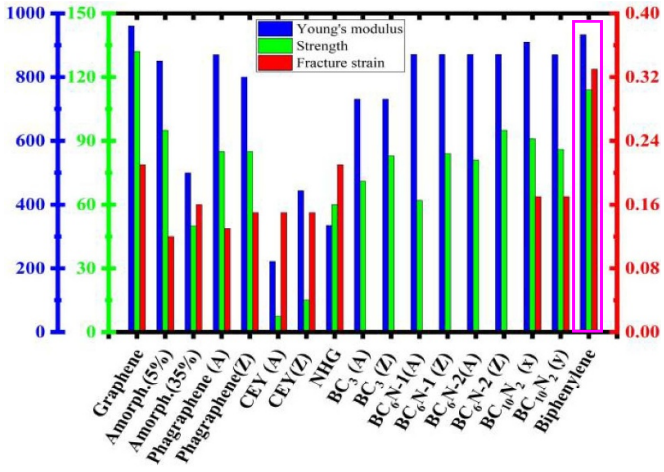

Figure 10. Comparison of mechanical properties among 2D carbon allotropes, B-C-N materials, and biphenylene, where the blue column represents Young's modulus (GPa), the green column represents tensile strength (GPa), and the red column represents fracture strain. (Reference: Graphene [74, [75], Amorph [75], Phagraphene [76], CEY [77], NHG [78], BC_3 [79], BC_6N-1 [79], BC_6N-2 [79], $BC_{10}N_2$ [80]).

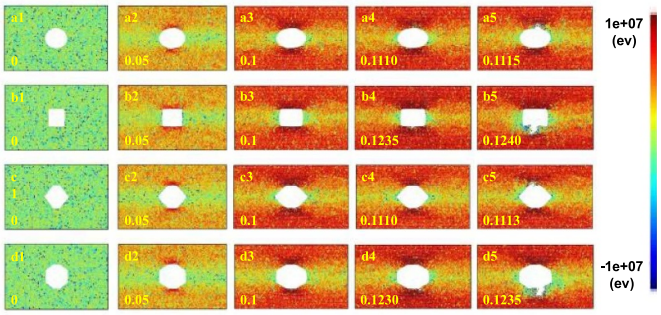

Figure 11. The evolution of stress at the atomic level throughout the stretching process. Each column corresponds to a strain state marked on the lower-left corner of each panel. Each row corresponds to the biphenylene embedded with one specific type of hole defect: the first row is for a circular hole with a diameter of 13 Å; the second row corresponds to a square hole with a side length of 13 Å; the third row represents a hexagonal hole with the farthest vertex distance of 20 Å; and the fourth row is for an octagonal hole with an opposite edge distance of 18 Å.

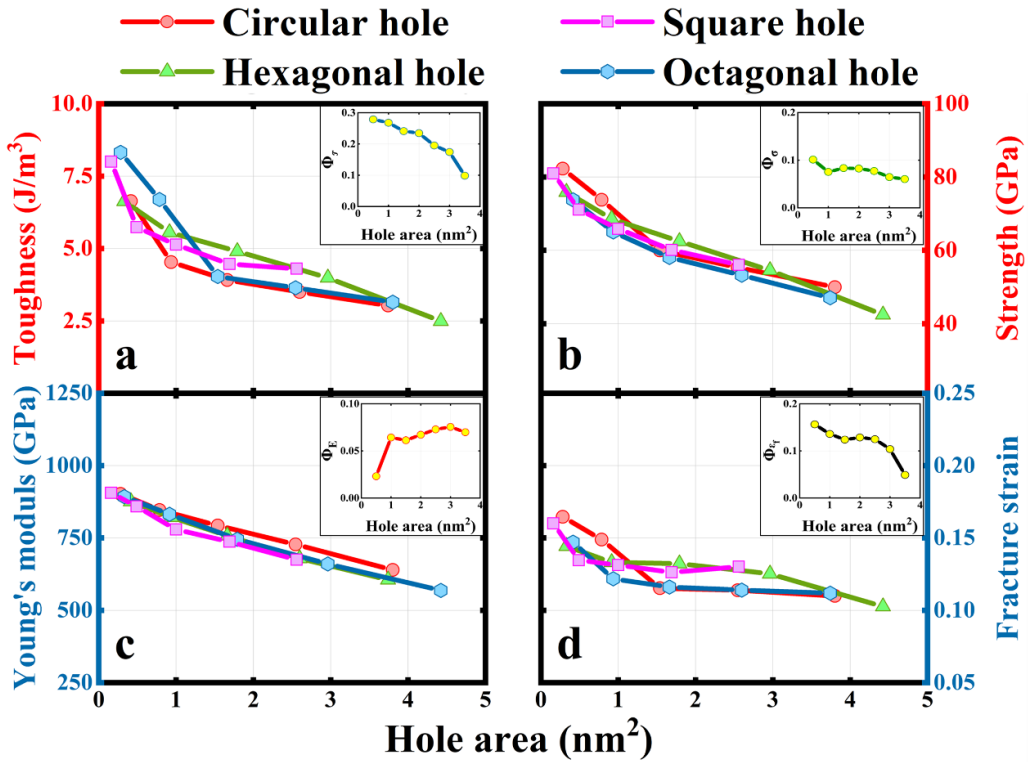

Figure 12. Superimposition of toughness (a), strength (b), Young's modulus (c), and fracture strain (d) versus the area of hole defects characterizing assorted shapes, including circles, squares, hexagons, and octagons. Φ_X(A) represents the spread of a relevant mechanical property at a given hole area, where X can be defined as E (Young's modulus), J (toughness), σ (strength), or ε_f (fracture strain).

the fracture mechanism seems to be independent of the shape of the hole defect under study.

Third, we investigated the impact of the defect dimensions on the mechanical properties. Because defects are characterized by various shapes, we employed the area rather than the length defined for each kind of defect previously. The results are superimposed together in figure 12. The derived quantities exhibit an almost consistent dependence on the area of the hole. To quantify the spread among curves, we define

$$\Phi_X(\mathrm{A}) = 2 \times \frac{X_{\max}(\mathbf{A}) - X_{\min}(\mathbf{A})}{X_{\max}(\mathbf{A}) + X_{\min}(\mathbf{A})}$$

where X represents the relevant mechanical properties at a given area of the hole defect regardless of the hole shape, denoted A. For Young's modulus and strength, the spread among the superimposed curves is relatively small, with Φ_X(A) values less than 10%. In contrast, for toughness and fracture strain, the spread among the superimposed curves is noticeably greater; however, with increasing hole size, the spread gradually decreases. These observations suggest that Young's modulus and strength depend only on the area of the hole, whereas toughness and fracture strain also depend on shape in addition to area.

5. Conclusions

In the present study, we have investigated the mechanical performance of pristine biphenylene and that embedded with various shapes and sizes of hole defects under uniaxial tension through molecular dynamics simulations. The pristine biphenylene has excellent mechanical properties. Moreover, we revealed that Young's modulus and strength depend only on the area of the defect, whereas fracture strain and toughness also depend on the shape of the hole in addition to its area. Furthermore, Young's modulus decreases linearly with increasing hole dimension, whereas the toughness, strength and fracture strain all exhibit nonlinear dependences. It would be interesting to investigate how these observations would evolve if different 2D materials were examined or if the shape and distribution of the hole defects were changed.

Data availability statement

The raw/processed data required to reproduce these findings cannot be shared at this time due to technical or time limitations.

All data that support the findings of this study are included within the article (and any supplementary files).

Acknowledgments

This work is supported by Strategic Priority Research Program of Chinese Academy of Sciences (Grant No. XDB0620103), National Natural Science Foundation of China (Grant No. 12272378), and High-level Innovation Research Institute Program of Guangdong Province (Grant No. 2020B0909010003).

Author contributions

S X: data curation, formal Analysis, investigation, software, supervision, validation, visualization, writing—original draft, writing—review & editing; J H: methodology, formal Analysis, figure plotting, writing—review & editing; T S: methodology, software, resources, writing—review & editing; J J: methodology, software, resources, writing—review & editing; B W: methodology, software, resources, Supervision, writing—review & editing. Q P: conceptualization, funding acquisition, methodology, project administration, software, resources, Supervision, writing—review & editing.

Conflict of interest

We declare that we do not have any commercial or associative interest that represents a conflict of interest in connection with the work submitted.

ORCID iDs

Jianfeng Jin https://orcid.org/0000-0002-0089-584X
Qing Peng https://orcid.org/0000-0002-8281-8636

References

[1] Tan C and Zhang H 2015 Two-dimensional transition metal dichalcogenide nanosheet-based composites *Chem. Soc. Rev.* **44** 2713–31
[2] Varghese S S, Varghese S H, Swaminathan S, Singh K K and Mittal V 2015 Two-dimensional materials for sensing: graphene and beyond *Electronics* **4** 651–87
[3] Shi E, Gao Y, Finkenauer B P, Akriti, Coffey A H, Dou L and Akriti A 2018 Two-dimensional halide perovskite nanomaterials and heterostructures *Chem. Soc. Rev.* **47** 6046–72
[4] Chhowalla M, Shin H S, Eda G, Li L-J, Loh K P and Zhang H 2013 The chemistry of two-dimensional layered transition metal dichalcogenide nanosheets *Nat. Chem.* **5** 263–75
[5] Dreyer D R, Park S, Bielawski C W and Ruoff R S 2009 The chemistry of graphene oxide *Chem. Soc. Rev.* **39** 228–40
[6] Tan C *et al* 2017 Recent advances in ultrathin two-dimensional nanomaterials *Chem. Rev.* **117** 6225–331
[7] Bhimanapati G R *et al* 2015 Recent advances in two-dimensional materials beyond graphene *ACS Nano* **9** 11509–39
[8] Butler S Z *et al* 2013 Progress, challenges, and opportunities in two-dimensional materials beyond graphene *ACS Nano* **7** 2898–926
[9] Payne M C, Teter M P, Allan D C, Arias T A and Joannopoulos J D 1992 Iterative minimization techniques for ab initio total-energy calculations: molecular dynamics and conjugate gradients *Rev. Mod. Phys.* **64** 1045–97
[10] Wang Q H, Kalantar-Zadeh K, Kis A, Coleman J N and Strano M S 2012 Electronics and optoelectronics of two-dimensional transition metal dichalcogenides *Nat. Nanotechnol.* **7** 699–712
[11] Mei H, Zhong Y, He D, Du X, Li C and Cheng N 2020 Elastic, electronic and optical properties of new 2D and 3D boron nitrides *Sci. Rep.* **10** 7873
[12] Park S and Ruoff R S 2009 Chemical methods for the production of graphenes *Nat. Nanotechnol.* **4** 217–24
[13] Dean C R *et al* 2010 Boron nitride substrates for high-quality graphene electronics *Nat. Nanotechnol.* **5** 722–6
[14] Li L, Yu Y, Ye G J, Ge Q, Ou X, Wu H, Feng D, Chen X H and Zhang Y 2014 Black phosphorus field-effect transistors *Nat. Nanotechnol.* **9** 372–7
[15] Novoselov K S, Fal′ko V I, Colombo L, Gellert P R, Schwab M G and Kim K 2012 A roadmap for graphene *Nature* **490** 192–200
[16] Shankar U, Oberoi D and Bandyopadhyay A 2022 A review on the alternative of indium tin oxide coated glass substrate in flexible and bendable organic optoelectronic device *Polym. Adv. Technol.* **33** 3078–111
[17] Xu M, Liang T, Shi M and Chen H 2013 Graphene-like two-dimensional materials *Chem. Rev.* **113** 3766–98
[18] Andrei E Y and MacDonald A H 2020 Graphene bilayers with a twist *Nat. Mater.* **19** 1265–75
[19] Zhu Y, Murali S, Cai W, Li X, Suk J W, Potts J R and Ruoff R S 2010 Graphene and graphene oxide: synthesis, properties, and applications *Adv. Mater.* **22** 3906–24
[20] Yang J *et al* 2019 Formation of two-dimensional transition metal oxide nanosheets with nanoparticles as intermediates *Nat. Mater.* **18** 970–6

[21] Mak K F, Lee C, Hone J, Shan J and Heinz T F 2010 Atomically thin MoS_2: a new direct-gap semiconductor *Phys. Rev. Lett.* **105** 136805

[22] Manzeli S, Ovchinnikov D, Pasquier D, Yazyev O V and Kis A 2017 2D transition metal dichalcogenides *Nat. Rev. Mater.* **2** 1–15

[23] Novoselov K S, Geim A K, Morozov S V, Jiang D, Zhang Y, Dubonos S V, Grigorieva I V and Firsov A A 2004 Electric field effect in atomically thin carbon films *Science* **306** 666–9

[24] Geim A K and Novoselov K S 2007 The rise of graphene *Nat. Mater.* **6** 183–91

[25] Novoselov K S, Geim A K, Morozov S V, Jiang D, Katsnelson M I, Grigorieva I V, Dubonos S V and Firsov A A 2005 Two-dimensional gas of massless Dirac fermions in graphene *Nature* **438** 197–200

[26] Castro Neto A H, Guinea F, Peres N M R, Novoselov K S and Geim A K 2009 The electronic properties of graphene *Rev. Mod. Phys.* **81** 109–62

[27] Zhang Y, Tan Y-W, Stormer H L and Kim P 2005 Experimental observation of the quantum Hall effect and Berry's phase in graphene *Nature* **438** 201–4

[28] Xia Y, Gao W and Gao C 2022 A review on graphene-based electromagnetic functional materials: electromagnetic wave shielding and absorption *Adv. Funct. Mater.* **32** 2204591

[29] Pham V-T and Fang T-H 2022 Mechanical and thermal characterizations of nanoporous two-dimensional boron nitride membranes *Sci. Rep.* **12** 6306

[30] Golberg D, Bando Y, Huang Y, Terao T, Mitome M, Tang C and Zhi C 2010 Boron nitride nanotubes and nanosheets *ACS Nano* **4** 2979–93

[31] Song L *et al* 2010 Large scale growth and characterization of atomic hexagonal boron nitride layers *Nano Lett.* **10** 3209–15

[32] Bonaccorso F, Colombo L, Yu G, Stoller M, Tozzini V, Ferrari A C, Ruoff R S and Pellegrini V 2015 Graphene, related two-dimensional crystals, and hybrid systems for energy conversion and storage *Science* **347** 1246501

[33] Fan Q *et al* 2021 Biphenylene network: a nonbenzenoid carbon allotrope *Science* **372** 852–6

[34] Luo Y, Ren C, Xu Y, Yu J, Wang S and Sun M 2021 A first principles investigation on the structural, mechanical, electronic, and catalytic properties of biphenylene *Sci. Rep.* **11** 19008

[35] Ren X, Wang K, Yu Y, Zhang D, Zhang G and Cheng Y 2023 Tuning the mechanical anisotropy of biphenylene by boron and nitrogen doping *Comput. Mater. Sci.* **222** 112119

[36] Bafekry A, Faraji M, Fadlallah M M, Jappor H R, Karbasizadeh S, Ghergherehchi M and Gogova D 2022 Biphenylene monolayer as a two-dimensional nonbenzenoid carbon allotrope: a first-principles study *J. Phys.: Condens. Matter* **34** 015001

[37] Xie Y, Chen L, Xu J and Liu W 2022 Effective regulation of the electronic properties of a biphenylene network by hydrogenation and halogenation *RSC Adv.* **12** 20088–95

[38] Shen H, Yang R, Xie K, Yu Z, Zheng Y, Zhang R, Chen L, Wu B-R, Su W-S and Wang S 2021 Electronic and optical properties of hydrogen-terminated biphenylene nanoribbons: a first-principles study *Phys. Chem. Chem. Phys.* **24** 357–65

[39] Wang K, Ren K, Zhang D, Cheng Y and Zhang G 2022 Phonon properties of biphenylene monolayer by first-principles calculations *Appl. Phys. Lett.* **121** 042203

[40] Hamed Mashhadzadeh A, Zarghami Dehaghani M, Molaie F, Fooladapanjeh S, Farzadian O and Spitas C 2022 A theoretical insight into the mechanical properties and phonon thermal conductivity of biphenylene network structure *Comput. Mater. Sci.* **214** 111761

[41] Samadian M, Ajri M, Azizi A and Hemmatpour-Khotbesara M A 2023 Investigating the pinhole effect on the mechanical properties of biphenylene *Appl. Phys.* A **129** 826

[42] Mortazavi B and Shapeev A V 2022 Anisotropic mechanical response, high negative thermal expansion, and outstanding dynamical stability of biphenylene monolayer revealed by machine-learning interatomic potentials *FlatChem* **32** 100347

[43] Hudspeth M A, Whitman B W, Barone V and Peralta J E 2010 Electronic properties of the biphenylene sheet and its one-dimensional derivatives *ACS Nano* **4** 4565–70

[44] Jiacheng Y, Li J, Zhong D Y and Yao D-X 2023 Possible superconductivity in biphenylene *Chin. Phys. Lett.* **40** 77401

[45] Ferguson D, Searles D J and Hankel M 2017 Biphenylene and phagraphene as lithium ion battery anode materials *ACS Appl. Mater. Interfaces* **9** 20577–84

[46] Zhao K, Pharr M, Vlassak J J and Suo Z 2010 Fracture of electrodes in lithium-ion batteries caused by fast charging *J. Appl. Phys.* **108** 073517

[47] Lu B, Ning C, Shi D, Zhao Y and Zhang J 2020 Review on electrode-level fracture in lithium-ion batteries* *Chin. Phys.* B **29** 026201

[48] Pereira M L, Da Cunha W F, De Sousa R T, Amvame Nze G D, Galvão D S and Ribeiro L A 2022 On the mechanical properties and fracture patterns of the nonbenzenoid carbon allotrope (biphenylene network): a reactive molecular dynamics study *Nanoscale* **14** 3200–11

[49] Peng Q, Ma Z, Cai S, Zhao S, Chen X and Cao Q 2023 Atomistic insights on surface quality control via annealing process in AlGaN thin film growth *Nanomaterials* **13** 1382

[50] Mortazavi B 2017 Ultra high stiffness and thermal conductivity of graphene like C3N *Carbon* **118** 25–34

[51] Huang X, Zhi C, Lin Y, Bao H, Wu G, Jiang P and Mai Y-W 2020 Thermal conductivity of graphene-based polymer nanocomposites *Mater. Sci. Eng.* R **142** 100577

[52] Peng Q, Meng F, Yang Y, Lu C, Deng H, Wang L, De S and Gao F 2018 Shockwave generates <100> dislocation loops in bcc iron *Nat. Commun.* **9** 4880

[53] Liu B and Zhou K 2019 Recent progress on graphene-analogous 2D nanomaterials: properties, modeling and applications *Prog. Mater. Sci.* **100** 99–169

[54] Wolf D, Yamakov V, Phillpot S R, Mukherjee A and Gleiter H 2005 Deformation of nanocrystalline materials by molecular-dynamics simulation: relationship to experiments? *Acta Mater.* **53** 1–40

[55] Zhan C, Lian C, Zhang Y, Thompson M W, Xie Y, Wu J, Kent P R C, Cummings P T, Jiang D and Wesolowski D J 2017 Computational insights into materials and interfaces for capacitive energy storage *Adv. Sci.* **4** 1700059

[56] Zhang Y, Li J, Hu Y, Ding S, Du F and Xia R 2022 Characterization of the deformation behaviors under uniaxial stress for bicontinuous nanoporous amorphous alloys *Phys. Chem. Chem. Phys.* **24** 1099–112

[57] Li Y, Wang Q and Wang S 2019 A review on enhancement of mechanical and tribological properties of polymer composites reinforced by carbon nanotubes and graphene sheet: molecular dynamics simulations *Composites* B **160** 348–61

[58] Habib M R, Liang T, Yu X, Pi X, Liu Y and Xu M 2018 A review of theoretical study of graphene chemical vapor deposition synthesis on metals: nucleation, growth, and the role of hydrogen and oxygen *Rep. Prog. Phys.* **81** 036501

[59] Yang J, Yang X and Li Y 2015 Molecular simulation perspective of liquid-phase exfoliation, dispersion, and stabilization for graphene *Curr. Opin. Colloid Interface Sci.* **20** 339–45

[60] Guo Z, Li X, Wang M and Cheng C 2023 Mechanical properties of Janus MoSSeNTs: a molecular dynamics simulation study *Mech. Mater.* **176** 104507
[61] Hou J, Deng B, Zhu H, Lan Y, Shi Y, De S, Liu L, Chakraborty P, Gao F and Peng Q 2019 Magic auxeticity angle of graphene *Carbon* **149** 350–4
[62] Fatema K N, Sagadevan S, Cho J Y, Jang W K and Oh W-C 2022 Graphene-based nanocomposite using new modeling molecular dynamic simulations for proposed neutralizing mechanism and real-time sensing of COVID-19 *Nanotechnol. Rev.* **11** 1555–69
[63] Thompson A P *et al* 2022 LAMMPS—a flexible simulation tool for particle-based materials modeling at the atomic, meso, and continuum scales *Comput. Phys. Commun.* **271** 108171
[64] Hirel P 2015 Atomsk: a tool for manipulating and converting atomic data files *Comput. Phys. Commun.* **197** 212–9
[65] Momma K and Izumi F 2011 *VESTA 3* for three-dimensional visualization of crystal, volumetric and morphology data *J. Appl. Crystallogr.* **44** 1272–6
[66] O'Connor T C, Andzelm J and Robbins M O 2015 AIREBO-M: a reactive model for hydrocarbons at extreme pressures *J. Chem. Phys.* **142** 024903
[67] Brenner D W, Shenderova O A, Harrison J A, Stuart S J, Ni B and Sinnott S B 2002 A second-generation reactive empirical bond order (REBO) potential energy expression for hydrocarbons *J. Phys.: Condens. Matter* **14** 783
[68] Stuart S J, Tutein A B and Harrison J A 2000 A reactive potential for hydrocarbons with intermolecular interactions *J. Chem. Phys.* **112** 6472–86
[69] Thamaraikannan S and Pradhan S C 2016 *TMS 2016 145th Annual Meeting & Exhibition* (Springer International Publishing) pp 293–300
[70] Peng Q, Huang Z, Chen G, Zhang Y, Zhang X, Chen X-J and Hu Z 2024 Effect of strain rate, temperature, vacancy, and microcracks on mechanical properties of 8-16-4 graphyne *Nanomaterials* **14** 556
[71] Koh S J A, Lee H P, Lu C and Cheng Q H 2005 Molecular dynamics simulation of a solid platinum nanowire under uniaxial tensile strain: temperature and strain-rate effects *Phys. Rev.* B **72** 085414
[72] Koh S J A and Lee H P 2006 Molecular dynamics simulation of size and strain rate dependent mechanical response of FCC metallic nanowires *Nanotechnology* **17** 3451
[73] Pereira L F C 2021 Investigating mechanical properties and thermal conductivity of 2D carbon-based materials by computational experiments *Comput. Mater. Sci.* **196** 110493
[74] Fan Z, Pereira L F C, Hirvonen P, Ervasti M M, Elder K R, Donadio D, Ala-Nissila T and Harju A 2017 Thermal conductivity decomposition in two-dimensional materials: application to graphene *Phys. Rev.* B **95** 144309
[75] Mortazavi B, Fan Z, Pereira L F C, Harju A and Rabczuk T 2016 Amorphized graphene: a stiff material with low thermal conductivity *Carbon* **103** 318–26
[76] Pereira L F C, Mortazavi B, Makaremi M and Rabczuk T 2016 Anisotropic thermal conductivity and mechanical properties of phagraphene: a molecular dynamics study *RSC Adv.* **6** 57773–9
[77] Mortazavi B, Shahrokhi M, Rabczuk T and Pereira L F C 2017 Electronic, optical and thermal properties of highly stretchable 2D carbon Ene-yne graphyne *Carbon* **123** 344–53
[78] Mortazavi B, Rahaman O, Rabczuk T and Pereira L F C 2016 Thermal conductivity and mechanical properties of nitrogenated holey graphene *Carbon* **106** 1–8
[79] Shahrokhi M, Raeisi M, Zhuang X, Pereira L F C and Rabczuk T 2019 Outstanding strength, optical characteristics and thermal conductivity of graphene -like BC3 and BC6N semiconductors *Carbon* **149** 733–42
[80] Tromer R M, Felix I M, Freitas A, Azevedo S and Pereira L F C 2020 Diboron-porphyrin monolayer: a new 2D semiconductor *Comput. Mater. Sci.* **172** 109338